J. Fluid Mech. (2012), *vol.* 699, *pp.* 500–510. © Cambridge University Press 2012
doi:10.1017/jfm.2012.146

Bottom-trapped currents as statistical equilibrium states above topographic anomalies

A. Venaille†

Laboratoire de Physique, ENS-Lyon, 46 Allée d'Italie, 69007 Lyon, France

(Received 10 January 2012; revised 27 February 2012; accepted 12 March 2012;
first published online 17 April 2012)

Oceanic geostrophic turbulence is mostly forced at the surface, yet strong bottom-trapped flows are commonly observed along topographic anomalies. Here we consider the case of a freely evolving, initially surface-intensified velocity field above a topographic bump, and show that the self-organization into a bottom-trapped current can result from its turbulent dynamics. Using equilibrium statistical mechanics, we explain this phenomenon as the most probable outcome of turbulent stirring. We compute explicitly a class of solutions characterized by a linear relation between potential vorticity and streamfunction, and predict when the bottom intensification is expected. Using direct numerical simulations, we provide an illustration of this phenomenon that agrees qualitatively with theory, although the ergodicity hypothesis is not strictly fulfilled.

Key words: geostrophic turbulence, quasi-geostrophic flows, topographic effects

1. Introduction

Bottom-intensified flows are commonly observed along topographic anomalies in the ocean. A striking example is given by the Zapiola anticyclone, a strong recirculation ∼500 km wide that takes place above a sedimentary bump in the Argentine Basin, where bottom-intensified velocities of the order of 0.1 m s^{-1} have been reported from *in situ* measurements (Saunders & King 1995) and models (de Miranda, Barnier & Dewar 1999). This bottom intensification may seem surprising, since the energy is mostly injected at the surface of the oceans (Ferrari & Wunsch 2009). Indeed, the primary source of geostrophic turbulence is mostly baroclinic instability, extracting turbulent energy from the potential energy reservoir set at the basin scale by large-scale wind patterns (Gill, Green & Simmons 1974), and involving surface-intensified unstable modes (see e.g. Smith 2007; Tulloch *et al.* 2011; Venaille, Vallis & Smith 2011*b*). This leads to the following question. How does a turbulent flow driven by surface forcing evolve into a bottom-intensified flow? A first necessary step to tackle this problem is to determine if an initially surface-intensified flow may evolve towards a bottom-intensified current without forcing and dissipation. Here we address this issue in the framework of freely evolving stratified quasi-geostrophic turbulence, which allows for theoretical analysis with equilibrium statistical mechanics.

The main idea of statistical mechanics is to predict the large-scale flow structure as the most probable outcome of turbulent stirring (Miller, Weichman & Cross 1992; Robert & Sommeria 1992). The interest in this approach is due to the possibility

† Email address for correspondence: antoine.venaille@ens-lyon.org

https://doi.org/10.1017/jfm.2012.146 Published online by Cambridge University Press

of computing this large-scale flow structure and studying its properties with respect to a few key parameters given by dynamical invariants (see e.g. Majda & Wang 2006; Bouchet & Venaille 2012). We focus here on a particular class of equilibrium states amenable to analytical treatment, namely those characterized by a linear relation between potential vorticity (PV) and streamfunction.

Phenomenological arguments for the formation of bottom-trapped flows have been given previously by Dewar (1998) in the forced–dissipated case. Here we provide a complementary point of view, built upon previous results of Merryfield (1998), who computed critical states of equilibrium statistical mechanics for truncated dynamics. He observed that some of these states were bottom-intensified in the presence of topography. Venaille, Vallis & Griffies (2012) showed how to find the equilibrium states among these critical states, and how they depend on the initial fine-grained enstrophy profile. However, they focused on the role of the beta effect in barotropization processes and did not discuss the effect of bottom topography. Here we show that bottom-trapped currents are actual statistical equilibria in the presence of sufficiently large bottom topography, and we present direct numerical simulations of the free evolution of an initial surface-intensified flow towards these bottom-trapped currents.

2. Equilibrium states of quasi-geostrophic flows

Here we consider an initial value problem for a Boussinesq, continuously stratified quasi-geostrophic fluid. Such flows are stably stratified with a prescribed buoyancy profile $N(z)$ above a topographic anomaly $h_b(x, y)$, and are strongly rotating at a rate $f_0/2$ such that $UL/f_0 \ll 1$, where U and L, respectively, are typical horizontal velocity and length of the flow. At leading order, the flow is at geostrophic balance: horizontal pressure gradients compensate the Coriolis term. The dynamics is then given by quasi-geostrophic equations (see Vallis 2006, § 5.4):

$$\partial_t q + \partial_x \psi \, \partial_y q - \partial_y \psi \, \partial_x q = 0, \tag{2.1}$$

$$q = \Delta \psi + \frac{\partial}{\partial z}\left(\frac{f_0^2}{N^2}\frac{\partial}{\partial z}\psi\right) + \beta y, \tag{2.2}$$

with

$$\partial_z \psi|_{z=0} = 0, \quad \left.\frac{f_0}{N^2}\partial_z \psi\right|_{z=-H} = -h_b, \tag{2.3}$$

where ψ is the streamfunction, Δ is the horizontal Laplacian and H is the ocean depth. We consider Cartesian coordinates, but the Earth's sphericity is taken into account at lowest order through the term βy, which is due to the meridional variations of the projection of the Earth's rotation rate on the local vertical axis. This is the beta plane approximation. The lateral buoyancy variations have been neglected in the upper and lower boundary conditions. The quasi-geostrophic approximation neglects topographic variations to leading order. This is why the term h_b appears only at the boundary $z = -H$.

The dynamics (2.1)–(2.3) takes place in three dimensions, but is expressed as the advection of a scalar field (the PV q) by a non-divergent horizontal velocity field, as in two-dimensional Euler dynamics. For this reason, the phenomenology of stratified quasi-geostrophic turbulence is similar to two-dimensional turbulence: there is an inverse energy cascade, self-organization at the domain scale and no dissipative anomaly.

https://doi.org/10.1017/jfm.2012.146 Published online by Cambridge University Press

Quasi-geostrophic dynamics develops complex PV filaments at finer and finer scales at each depth z, associated with a forward cascade of enstrophy (Kraichnan & Montgomery 1980). Rather than describing the fine-grained structures, equilibrium statistical theories of two-dimensional turbulent flows, by assuming ergodicity (or at least sufficient mixing in phase space, corresponding to stirring in physical space), predict self-organization of the flow on a coarse-grained level (Miller *et al.* 1992; Robert & Sommeria 1992, hereafter MRS): a 'mixing entropy' is maximized by taking into account the constraints, namely, all the flow invariants, which are the total energy

$$\mathscr{E} = \frac{1}{2}\int_{-H}^{0} \mathrm{d}z \int_{\mathscr{D}} \mathrm{d}x\,\mathrm{d}y \left[(\nabla\psi)^2 + \frac{f_0^2}{N^2}(\partial_z\psi)^2\right] \tag{2.4}$$

and the Casimir functionals $\mathscr{C}_g(z)[q] = \int_{\mathscr{D}} \mathrm{d}x\,\mathrm{d}y\, g(q)$, where g is any continuous function, and $\mathscr{D}$ the domain where the flow takes place. Here we consider the case of a doubly periodic domain. In the case $g(q) = q^2/2$, $\mathscr{C}_g$ is the enstrophy. The output of the theory is a coarse-grained PV field $\overline{q}$, obtained by locally averaging the fine-grained PV field q.

Let us call $E_0 = \mathscr{E}(q_0)$ and $Z_0(z) = \frac{1}{2}\int_{\mathscr{D}} \mathrm{d}x\,\mathrm{d}y\, q_0^2$ the energy and fine-grained enstrophy, respectively, of the initial condition given by $q_0(x, y, z)$. Using a general result of Bouchet (2008), it is shown in Venaille *et al.* (2012, appendix 1) that, in the *low-energy limit*, the calculation of MRS equilibrium states amounts to finding the minimizer $\overline{q}_{min}$ of the 'total coarse-grained enstrophy'

$$\mathscr{Z}_{cg}^{tot}[\overline{q}] = \frac{1}{2}\int_{-H}^{0} \mathrm{d}z \int_{\mathscr{D}} \mathrm{d}x\,\mathrm{d}y\, \frac{\overline{q}^2}{Z_0} \tag{2.5}$$

among all the fields $\overline{q}$ satisfying the energy constraint

$$\mathscr{E}[\overline{q}] = \frac{1}{2}\int_{\mathscr{D}} \mathrm{d}x\,\mathrm{d}y\, f_0 h_b \psi|_{z=-H} - \frac{1}{2}\int_{\mathscr{D}} \mathrm{d}x\,\mathrm{d}y \int_{-H}^{0} \mathrm{d}z\,(\overline{q} - \beta y)\psi = E_0, \tag{2.6}$$

where (2.6) is obtained after integrating (2.4) by parts. Independently of the statistical mechanics arguments, the variational problem (2.5)–(2.6) can be seen as a generalization to the stratified case of the phenomenological minimum enstrophy principle of Bretherton & Haidvogel (1976). Besides, these states are statistical equilibria of the truncated dynamics (Salmon, Holloway & Hendershott 1976; Kraichnan & Montgomery 1980) in the limit of infinite wavenumber cut-off (Carnevale & Frederiksen 1987).

Critical states of the variational problem (2.5)–(2.6) are computed by introducing a Lagrange multiplier β_t associated with the energy constraint (which should not be confused with the beta effect), and by solving $\delta\mathscr{Z}_{cg}^{total} + \beta_t\delta\mathscr{E} = 0$, where variations of the functionals are taken with respect to $\overline{q}$, leading to the linear relation $\overline{q} = \beta_t Z_0\psi$ (see also Venaille *et al.* 2012). The next step is to find which of these critical states are actual minimizers of the coarse-grained enstrophy for a given energy.

3. Analytical calculations and simulations

We consider the configuration of figure 1(*a*): the stratification is linear in the bulk (N is constant for $-H + h < z < -h$), and homogeneous in two layers of thickness $h \ll H$ at the top and at the bottom, where $N = 0^+$. In these upper and lower layers, the streamfunction is depth-independent, denoted by $\psi^{top}(x, y, t)$ and $\psi^{bot}(x, y, t)$, respectively. In these layers, the dynamics is then fully described by the advection

https://doi.org/10.1017/jfm.2012.146 Published online by Cambridge University Press

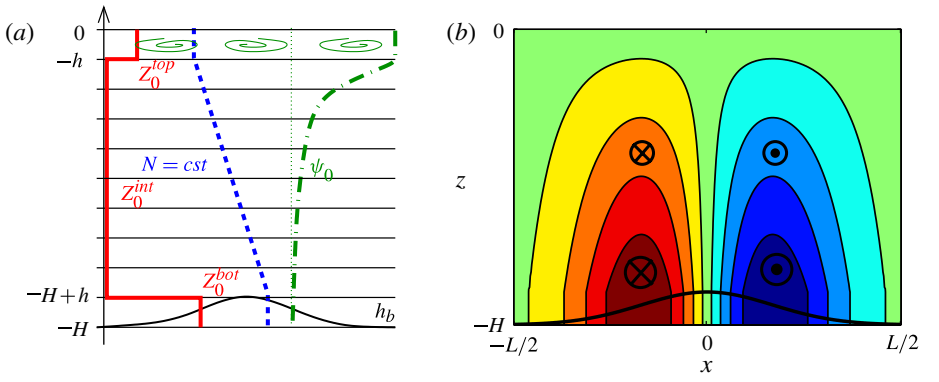


FIGURE 1. (Colour online available at journals.cambridge.org/flm) (*a*) Sketch of the flow configuration. The continuous dark grey (red online) line represents the initial fine-grained enstrophy profile (here $Z_0^{int} = 0$, as assumed in the Appendix). The dashed dark grey (blue) line represents the density profile, and the dashed-dotted grey (green) line represents the streamfunction amplitude shape, which is initially surface-intensified. The continuous thick black line represents bottom topography. (*b*) Vertical slice of the meridional velocity field v of the statistical equilibrium state in the low-energy limit.

of the vertical average of the PV fields, denoted by $q^{top}(x, y, t)$ and $q^{bot}(x, y, t)$. The interior PV field is denoted by $q^{int}(x, y, z, t)$. For a given field q^{top}, q^{int} and q^{bot}, the streamfunction is obtained by inverting the following equations:

$$q^{top} - \beta y = \Delta\psi^{top} - \frac{f_0^2}{hN^2}\frac{\partial}{\partial z}\psi\bigg|_{z=-h}, \tag{3.1}$$

$$q^{bot} - \beta y - f_0\frac{h_b}{h} = \Delta\psi^{bot} + \frac{f_0^2}{hN^2}\frac{\partial}{\partial z}\psi\bigg|_{z=h-H}, \tag{3.2}$$

$$q^{int} - \beta y = \Delta\psi + \frac{f_0^2}{N^2}\frac{\partial^2}{\partial z^2}\psi \quad \text{for} \quad -H + h < z < -h, \tag{3.3}$$

$$\psi^{top} = \psi(x, y, -h), \quad \psi^{bot} = \psi(x, y, -H + h). \tag{3.4}$$

Equations (3.1) and (3.2) are obtained by averaging (2.2) in the vertical direction in the upper and lower layers, respectively, and by using the boundary condition (2.3). In the following, the initial condition is a surface-intensified velocity field induced by a perturbation of the PV field confined in the upper layer:

$$q_0^{top} = \beta y + q_0^{pert}, \quad q_0^{int} = \beta y, \quad q_0^{bot} = \frac{f_0}{h}h_b + \beta y. \tag{3.5}$$

It is assumed in the following that $\beta y \ll q_0^{pert} \ll f_0 h_b/h$. The PV fields are therefore associated with fine-grained enstrophies $Z_0^{int} \ll Z_0^{top} \ll Z_0^{bot}$. We compute in the Appendix the coarse-grained enstrophy minimizers of this configuration by solving the variational problem (2.5)–(2.6). The main result is that, for a fixed topography, in the *low-energy limit*, the equilibrium streamfunction is a bottom-intensified quasi-geostrophic flow such that bottom streamlines follow contours of topography with positive correlations (see figure 1*b*). Given the choice of our initial condition, considering the low-energy limit for a fixed topography is equivalent to considering a large-topography limit for a fixed energy.

https://doi.org/10.1017/jfm.2012.146 Published online by Cambridge University Press

We perform simulations of the dynamics by considering a horizontal discretization of 512^2 in a doubly periodic square domain of size $L = 2\pi$, and a vertical discretization with 10 layers of equal depth $h = 0.1$, using a pseudo-spectral quasi-geostrophic model (Smith & Vallis 2001). The linearly stratified region of figure 1 is therefore approximated by eight layers of depth h. We present results without small-scale dissipation, but we checked that adding a weak enstrophy filter or hyperviscosity did not change the results qualitatively.

The perturbation q_0^{pert} of the PV field in the upper layer has random phases in spectral space with a Gaussian power spectrum peaked at wavenumber $K_0 = 5$, with variance $\delta K_0 = 2$, and normalized such that the total energy is equal to one ($E_0 = 1$), the latter amounting to a rescaling of time. The bottom topography h_b is a Gaussian bump of amplitude H_b and of typical width $\sigma = L/2$. There are three independent parameters:

$$\text{(i)}\ \frac{L_d}{L} = \frac{NH}{2f_0 L}, \quad \text{(ii)}\ \frac{L_\beta}{L} = \frac{1}{L}\left(\frac{V_0}{\beta}\right)^{1/2}, \quad \text{(iii)}\ \frac{L_{h_b}}{L} = \frac{1}{L^{1/2}}\left(\frac{hV_0}{2f_0 H_B}\right)^{1/2}, \tag{3.6}$$

where $V_0 = (E_0/L^2 H)^{1/2}$ is an estimate for the velocity. The first parameter is the ratio between the first baroclinic radius of deformation and the domain scale, taken to be $L_d/L = 1/10$. The second one is the ratio between the Rhines scale and the domain scale. We choose $L_\beta/L = 1/3$. The third one is the ratio of a topographic Rhines scale to the domain scale, taken to be $L_{h_b}/L = 1/10$. We show in the Appendix that the latter choice is consistent with the low-energy or large-topography limit considered in the previous section. The choices of β and H_b are also consistent with the hypothesis that $Z_0^{int} \ll Z_0^{top} \ll Z_0^{bot}$. The choice $K_0 = 6$ for the initial condition is motivated by the fact that, in the forced–dissipated case, the energy is injected through baroclinic instability with a most unstable mode having a wavelength of a few Rossby wavelengths of deformation (see e.g. Vallis 2006; Smith 2007). We checked that changing this initial horizontal length scale did not change the results.

We see in figure 2(*b*) that the initial condition resembles a classical surface quasi-geostrophic mode (Held *et al.* 1995). After a few eddy turnover times, the enstrophy of the upper layer has cascaded towards small scales as shown by numerous filaments in figure 2(*c*), concomitantly with an increase of the horizontal energy length scale. The projection of a surface quasi-geostrophic mode on a Fourier mode of wavenumber K is characterized by a typical e-folding depth of f_0/NK on the vertical. The inverse energy cascade on the horizontal leads therefore to a deeper penetration of the velocity field, shown in figure 2(*d*). When this velocity field reaches the bottom layer, it starts to stir the bottom PV field. This induces a bottom-intensified flow, which then stirs the surface PV field, and so on. The flow reaches a stationary state after a few dozen eddy turnover times: the $\overline{q}$–ψ relation in each layer converges towards a well-defined functional relation after coarse graining. The existence of this functional relation implies $\partial_t \overline{q} = 0$, meaning that there are no temporal fluctuations. The corresponding flow is shown in figure 2(*e*), which clearly represents a bottom-intensified anticyclonic flow above the topographic anomaly, qualitatively similar to the one predicted by statistical mechanics in the low-energy limit. However, we observe the formation of multiple jets (here two) around the topographic bump, as in Vallis & Maltrud (1993), which indicates that the 'sufficient stirring' hypothesis is not strictly fulfilled in the simulations. In addition, the observed $\overline{q}$–ψ relations are monotonic, as expected from MRS theory, but not strictly linear, as would have been expected in the low-energy limit. The theoretical results obtained in the linear

https://doi.org/10.1017/jfm.2012.146 Published online by Cambridge University Press

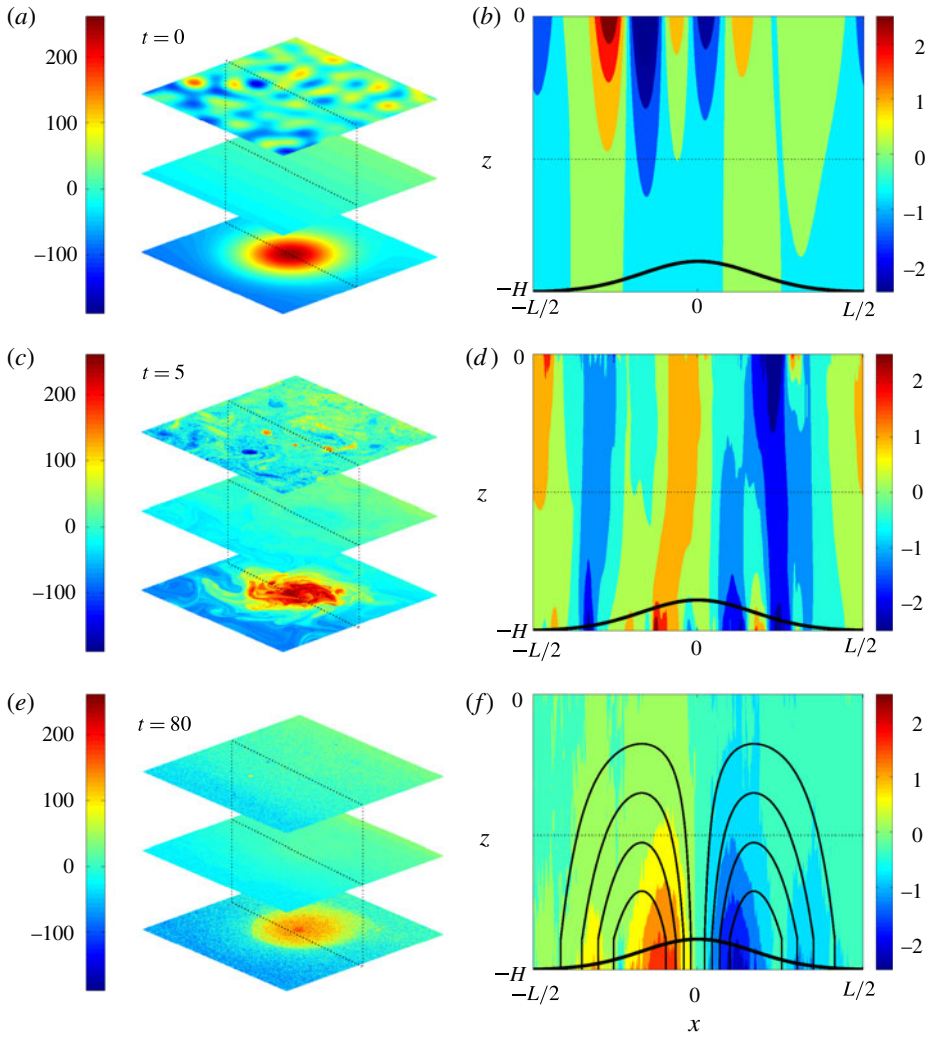


FIGURE 2. (Colour online) (*a*,*c*,*e*) PV field at three successive times. In each figure, only layers 1 (top), 5 (middle) and 10 (bottom) are represented. (*b*,*d*,*f*) Vertical slices of the meridional velocity fields v taken at the centre of the domain ($y = 0$), and associated with the PV fields given in panels (*a*,*c*,*e*), respectively. The continuous thick black line represents the bottom topography. The continuous black contours in panel (*f*) give the structure of the statistical equilibrium state in the low-energy (or large-topography) limit, corresponding to figure 1(*b*). Contour intervals are the same as those between the different shades (colours).

case provide a qualitative understanding of the observed vertical flow structure, but taking into account higher-order invariants than the fine-grained enstrophy will be necessary for quantitative comparisons between numerical simulations and statistical mechanics predictions. These higher-order invariants are indeed required to account for nonlinearities in the $\overline{q}$–ψ relations.

The same evolution from a surface-intensified turbulent field towards a bottom-trapped flow was observed in the absence of a beta effect, except that there remained two small surface-intensified coherent vortices locked above the topography extrema.

https://doi.org/10.1017/jfm.2012.146 Published online by Cambridge University Press

These vortices are destroyed by radiation of Rossby waves in the presence of β, as in Maltrud & Vallis (1991). In a way, small values of β enhance PV stirring, even if they have a negligible effect on the structure of the equilibrium state. However, if β is too large, then $L_\beta \ll L_{h_b}$, which leads to zonal jets that prevent the formation of bottom-trapped flow along topographic anomalies.

4. Conclusion

For sufficiently large values of bottom topography, statistical mechanics predicts that an initially surface-intensified velocity field will evolve towards a bottom-intensified flow following contours of topography. To the best of our knowledge, this is the first analytical calculation of statistical equilibrium states for stratified quasi-geostrophic equations above topography, although there have been many works on one- or few-layer models (see e.g. Majda & Wang 2006), and also critical states were computed by Merryfield (1998) in the stratified case. We chose to present these calculations in the simplest possible setting in order to give the main physical ideas. We found qualitative agreement between statistical mechanics predictions and a direct numerical simulation of the freely evolving dynamics.

The statistical mechanics approach highlights the crucial role of energy and fine-grained enstrophy conservation (among other invariants) while taking into account the turbulent nature of the dynamics. Here we considered the equilibrium states characterized by energy and enstrophy only, which is justified in the low-energy limit, and which leads to linear $\overline{q}$–ψ relations. The next step will be to consider higher-order invariants, in order to account for equilibrium states associated with nonlinear $\overline{q}$–ψ relations; see e.g. Bouchet & Simonnet (2009) in the context of Euler equations.

The main shortcoming of the statistical mechanics approach is that it predicts only the final state organization, and not how the system evolves towards this state. In addition, there remain quantitative discrepancies between theory and simulations, because the ergodicity, or 'sufficient stirring' hypothesis may not be strictly fulfilled in some cases. Addressing specifically the range of parameters for which the statistical mechanics predictions are accurate, and estimating how the relaxation time towards equilibrium depends on these parameters will be the object of a future work.

These results have important consequences for ocean energetics: topographic anomalies allow surface-intensified eddy kinetic energy to be transferred into bottom-trapped mean kinetic energy, which would eventually be dissipated in the presence of bottom friction, as, for instance in the case of the Zapiola anticyclone (Dewar 1998; Venaille *et al.* 2011*a*). In the case of the Zapiola anticyclone, the dissipation time scale is of the order of a few eddy turnover times. It is therefore not *a priori* obvious that the results obtained in a freely evolving configuration may apply to this case. However, we consider that it was a necessary first step. One can now build upon these results to address the role of forcing and dissipation in vertical energy transfers above topographic anomalies.

Acknowledgements

Most of this work was supported by DoE grant DE-SC0005189, by NOAA grant NA08OAR4320752 and by the contract LORIS (ANR-10-CEXC-010-01). Warm thanks are due to F. Bouchet, S. Griffies, I. Held, J. Le Sommer, J. Sommeria and G. Vallis for fruitful discussions and inputs. The author also thanks K .S. Smith for sharing his QG code, and J. Laurie and S. Gupta for useful comments on the

https://doi.org/10.1017/jfm.2012.146 Published online by Cambridge University Press

manuscript. The presentation of the results has been significantly improved thanks to the very detailed comments of an anonymous reviewer.

Appendix. Calculation of the solution

We compute statistical equilibria for the configuration sketched in figure 1 and detailed in § 3, by applying a general method presented in Venaille & Bouchet (2011). Here we consider the limit of small beta effect. The case without topography but including the beta effect is discussed in Venaille *et al.* (2012).

When $\beta \to 0$, only the upper and lower layers are dynamically active. The reason is that the interior fine-grained enstrophy tends to zero. We have seen in § 2 that a solution of the variational problem (2.5)–(2.6) necessarily satisfies $\overline{q} = \beta_t Z_0 \psi$. This gives $\int_{\mathscr{D}} \mathrm{d}x\,\mathrm{d}y\,\overline{q}^2/Z_0 \sim Z_0$. We conclude that $\lim_{Z_0 \to 0^+} \int_{\mathscr{D}} \mathrm{d}x\,\mathrm{d}y\,\overline{q}^2/Z_0 = 0$. The variational problem (2.5)–(2.6) therefore amounts to finding the minimizers of

$$\mathscr{Z}_{cg}^{tot}[\overline{q}^{top}, \overline{q}^{bot}] = \frac{1}{2}\frac{h}{Z_0^{top}} \int_{\mathscr{D}} \mathrm{d}x\,\mathrm{d}y\ (\overline{q}^{top})^2 + \frac{1}{2}\frac{h}{Z_0^{bot}} \int_{\mathscr{D}} \mathrm{d}x\,\mathrm{d}y\ (\overline{q}^{bot})^2, \tag{A 1}$$

with the constraint that

$$\mathscr{E}[\overline{q}^{top}, \overline{q}^{bot}] = -\frac{h}{2} \int_{\mathscr{D}} \mathrm{d}x\,\mathrm{d}y\,\overline{q}^{top}\psi^{top} - \frac{h}{2} \int_{\mathscr{D}} \mathrm{d}x\,\mathrm{d}y \left(\overline{q}^{bot} - f_0 \frac{h_b}{h}\right) \psi^{bot} = E_0. \tag{A 2}$$

One could also derive this variational problem directly from the MRS variational problem, using the method presented in the appendix of Venaille *et al.* (2012), and assuming that PV levels are zero everywhere except in the lower and upper homogeneous layers.

In order to solve the variational problem (A 1)–(A 2), we use the fact that any minimizer $\overline{q}^{top}_{\beta_t}$, $\overline{q}^{bot}_{\beta_t}$ of the 'free energy' $\mathscr{F} = \mathscr{Z}_{cg}^{tot} + \beta_t \mathscr{E}$ is a minimizer of the enstrophy $\mathscr{Z}_{cg}^{tot}$ with the energy constraint $E_{\beta_t} = \mathscr{E}[\overline{q}^{top}_{\beta_t}, \overline{q}^{bot}_{\beta_t}]$ (see e.g. Venaille & Bouchet 2011, and references therein).

The first step is to compute the free energy. For that purpose, it is convenient to consider Fourier modes $\psi = \sum_{k,l} \widehat{\psi}_{k,l} \exp(\mathrm{i}kx + \mathrm{i}ly)$ and solve (3.3)–(3.4) for each Fourier component:

$$\left.\begin{aligned} &\widehat{\psi}_{k,l}(z) = \widehat{\psi}^{top}_{k,l} \frac{\sinh(z + H/\lambda_K)}{\sinh(H/\lambda_K)} - \widehat{\psi}^{bot}_{k,l} \frac{\sinh(z/\lambda_K)}{\sinh(H/\lambda_K)}, \quad \lambda_K = \frac{f_0}{NK}, \\ &K = (k^2 + l^2)^{1/2}, \end{aligned}\right\} \tag{A 3}$$

where we have considered the limit $h \ll H$ to simplify the expressions. Each Fourier component of the streamfunction is a linear combination of a surface quasi-geostrophic mode and a bottom-trapped quasi-geostrophic mode. Substitution of (A 3) into the Fourier projections of (3.1)–(3.2) yields

$$\widehat{\overline{q}}^{top}_{k,l} = a_K \widehat{\psi}^{top}_{k,l} + b_K \widehat{\psi}^{bot}_{k,l}, \quad \widehat{\overline{q}}^{bot}_{k,l} = b_K \widehat{\psi}^{top}_{k,l} + a_K \widehat{\psi}^{bot}_{k,l} + \frac{f_0}{h} (\widehat{h}_b)_{k,l}, \tag{A 4}$$

with

$$a_K = -K^2 \left(1 + \frac{\lambda_K}{h \tanh(H/\lambda_K)}\right), \quad b_K = K^2 \frac{\lambda_K}{h \sinh(H/\lambda_K)}. \tag{A 5}$$

In order to compute the free energy $\mathscr{F} = \mathscr{Z}_{cg}^{tot} + \beta_t \mathscr{E}$, we first express the enstrophy (A 1) and the energy (A 2) in terms of the Fourier components of the

https://doi.org/10.1017/jfm.2012.146 Published online by Cambridge University Press

streamfunction, PV fields and bottom topography. We finally use (A 4) to express the streamfunction in terms of the PV fields and the topography, which yields

$$\mathscr{F} = \frac{h}{2}\sum_{k,l}\left(\left(\frac{1}{Z_0^{top}}+\frac{\beta_t a_K}{a_K^2-b_K^2}\right)\left(\widehat{\overline{q}}^{top}_{k,l}\right)^2+\left(\frac{1}{Z_0^{bot}}+\frac{\beta_t a_K}{a_K^2-b_K^2}\right)\left(\widehat{\overline{q}}^{bot}_{k,l}-\frac{f_0}{h}\left(\widehat{h}_b\right)_{k,l}\right)^2\right)$$
$$+\frac{h}{2}\sum_{k,l}\left(\frac{2\beta_t b_K}{a_K^2-b_K^2}\widehat{\overline{q}}^{top}_{k,l}\left(\widehat{\overline{q}}^{bot}_{k,l}-\frac{f_0}{h}\left(\widehat{h}_b\right)_{k,l}\right)\right). \tag{A 6}$$

After some manipulations, we find that the quadratic part of $\mathscr{F}$ is positive definite for $\beta_t \in (\beta_t^{min}, +\infty)$, where β_t^{min} is the largest root of $(\beta_t Z_0^{top} - a_1)(\beta_t Z_0^{bot} - a_1) = b_1^2$, implying that there exists a unique minimizer for each $\beta_t \in (\beta_t^{min}, +\infty)$. In addition, there is at least one unstable (negative) direction for $\mathscr{F}$ when $\beta_t \in (-\infty, \beta_t^{min})$, implying that there is no minimizer for this range of parameters.

When it exists, the minimizer $\overline{q}_{min}$ of the functional $\mathscr{F}$ can be explicitly computed for each value of β_t. The first step is to compute the critical points of the functional, which are solutions of $\delta\mathscr{F} = \delta\mathscr{Z}_{cg}^{tot} + \beta_t\delta\mathscr{E} = 0$, where variations are taken with respect to the PV fields $\overline{q}^{bot}$ and $\overline{q}^{top}$. This leads to $\overline{q}^i = \beta_t Z_0^i \psi^i$ with $i \in \{bot, top\}$. Substituting the Fourier projections of these expressions in (A 4) yields

$$\widehat{\psi}^{top}_{k,l} = \frac{f_0}{h}\frac{b_K}{(\beta_t Z_0^{top}-a_K)(\beta_t Z_0^{bot}-a_K)-b_K^2}\left(\widehat{h}_b\right)_{k,l}, \quad \widehat{\psi}^{bot}_{k,l} = \frac{\beta_t Z_0^{top}-a_K}{b_K}\widehat{\psi}^{top}_{k,l}. \tag{A 7}$$

For a given non-zero topography, the energy tends to zero when $\beta_t \to +\infty$, and tends to infinity when $\beta_t \to \beta_t^{min}$. It is therefore possible to reach any admissible energy by varying the inverse temperature between β_t^{min} and $+\infty$. It thus means that we have found all the energy–enstrophy statistical equilibria.

Let us first consider the limit $\beta_t Z_0^{bot} L^2 \to +\infty$. The solution (A 7) tends to

$$\widehat{\psi}^{top}_{k,l} \approx \frac{f_0 b_K \left(\widehat{h}_b\right)_{k,l}}{(h\beta_t^2 Z_0^{top} Z_0^{bot})}, \quad \widehat{\psi}^{bot}_{k,l} \approx \frac{f_0\left(\widehat{h}_b\right)_{k,l}}{h\beta_t Z_0^{bot}}. \tag{A 8}$$

We see that $\psi^{bot} = f_0 h_b/(h\beta_t Z_0^{bot})$ is along contours of topography, and that the vertical structure of the equilibrium state is dominated by the bottom-trapped quasi-geostrophic mode, since $\psi^{top} \ll \psi^{bot}$. Using the energy expression (2.4), we obtain $E_0 \sim HL^2\left(f_0 H_b/Lh\beta_t Z_0^{bot}\right)^2$, and substituting this expression in ((3.6)iii) yields $\beta_t Z_0 L^2 \sim (L/L_{h_b})^2$. These estimates explain *a posteriori* the term *low-energy limit* or *large-topography limit* when $\beta_t Z_0^{bot} L^2 \to +\infty$, and the fact that this limit corresponds to $L_{h_b} \ll L$.

In the *low-topography limit* or *large-energy limit*, the ratio Z_0^{bot}/Z_0^{top} tends to zero, and we deduce from (A 7) that $\beta_t \approx \beta_t^{min} \approx (a_1 - b_1^2/a_1)/Z_0^{top}$, which implies that ψ^{top} is dominated by its Fourier component on the horizontal mode $K = 1$. We also deduce from (A 7) that $\psi^{bot} \approx -(b_1/a_1)\psi^{top} \ll \psi^{top}$: the equilibrium state is a surface quasi-geostrophic mode. We have thus described a class of equilibrium states varying from a surface quasi-geostrophic mode condensed in the gravest Laplacian eigenmode (*low-topography limit* or *large-energy limit*) to a bottom-trapped quasi-geostrophic mode following contours of topography (*low energy limit* or *large-topography limit*). In the framework of MRS theory, only the low-energy limit is consistent with the derivation of the quadratic variational problem (A 1)–(A 2).

https://doi.org/10.1017/jfm.2012.146 Published online by Cambridge University Press

Finally, the numerical simulations were performed with ten homogeneous layers, which is a slightly different case from that studied in this appendix, with linear interior stratification. However, the present analytical results easily generalize to arbitrary stable interior stratification profiles. We do not expect different qualitative behaviours for the equilibrium states, although the convergence towards equilibrium may depend on stratification properties.

REFERENCES

BOUCHET, F. 2008 Simpler variational problems for statistical equilibria of the 2D Euler equation and other systems with long range interactions. *Physica* D: *Nonlinear Phenom.* **237**, 1976–1981.

BOUCHET, F. & SIMONNET, E. 2009 Random changes of flow topology in two-dimensional and geophysical turbulence. *Phys. Rev. Lett.* **102** (9), 094504.

BOUCHET, F. & VENAILLE, A. 2012 Statistical mechanics of two-dimensional and geophysical flows. *Phys. Rep.*, doi:10.1016/j.physrep.2012.02.001.

BRETHERTON, F. P. & HAIDVOGEL, D. B. 1976 Two-dimensional turbulence above topography. *J. Fluid Mech.* **78**, 129–154.

CARNEVALE, G. F. & FREDERIKSEN, J. S. 1987 Nonlinear stability and statistical mechanics of flow over topography. *J. Fluid Mech.* **175**, 157–181.

DEWAR, W. K. 1998 Topography and barotropic transport control by bottom friction. *J. Mar. Res.* **56**, 295–328.

FERRARI, R. & WUNSCH, C. 2009 Ocean circulation kinetic energy: reservoirs, sources, and sinks. *Annu. Rev. Fluid Mech.* **41**, 253–282.

GILL, A. E., GREEN, J. S. A. & SIMMONS, A. J. 1974 Energy partition in the large-scale ocean circulation and the production of mid-ocean eddies. *Deep-Sea Res.* **21**, 499–528.

HELD, I. M., PIERREHUMBERT, R. T., GARNER, S. T. & SWANSON, K. L. 1995 Surface quasi-geostrophic dynamics. *J. Fluid Mech.* **282**, 1–20.

KRAICHNAN, R. H. & MONTGOMERY, D. 1980 Two-dimensional turbulence. *Rep. Prog. Phys.* **43**, 547–619.

MAJDA, A. & WANG, X. 2006 *Nonlinear Dynamics and Statistical Theories for Basic Geophysical Flows*. Cambridge University Press.

MALTRUD, M. & VALLIS, G. K. 1991 Energy spectra and coherent structures in forced two-dimensional and geostrophic turbulence. *J. Fluid Mech.* **228**, 321–342.

MERRYFIELD, W. J. 1998 Effects of stratification on quasi-geostrophic inviscid equilibria. *J. Fluid Mech.* **354**, 345–356.

MILLER, J., WEICHMAN, P. B. & CROSS, M. C. 1992 Statistical mechanics, Euler's equation, and Jupiter's red spot. *Phys. Rev.* A **45**, 2328–2359.

DE MIRANDA, A. P., BARNIER, B. & DEWAR, W. K. 1999 On the dynamics of the Zapiola anticyclone. *J. Geophys. Res.* **104**, 21137–21150.

ROBERT, R. & SOMMERIA, J. 1992 Relaxation towards a statistical equilibrium state in two-dimensional perfect fluid dynamics. *Phys. Rev. Lett.* **69**, 2776–2779.

SALMON, R., HOLLOWAY, G. & HENDERSHOTT, M. C. 1976 The equilibrium statistical mechanics of simple quasi-geostrophic models. *J. Fluid Mech.* **75**, 691–703.

SAUNDERS, P. M. & KING, B. A. 1995 Bottom currents derived from a shipborne ADCP on WOCE cruise A11 in the South Atlantic. *J. Phys. Oceanogr.* **25**, 329–347.

SMITH, K. S. 2007 The geography of linear baroclinic instability in Earth's oceans. *J. Mar. Res.* **65**, 655–683.

SMITH, K. S. & VALLIS, G. K. 2001 The scales and equilibration of midocean eddies: freely evolving flow. *J. Phys. Oceanogr.* **31**, 554–571.

TULLOCH, R., MARSHALL, J., HILL, C. & SMITH, K. S. 2011 Scales, growth rates and spectral fluxes of baroclinic instability in the ocean. *J. Phys. Oceanogr.* **41**, 1057–1076.

VALLIS, G. K. 2006 *Atmospheric and Oceanic Fluid Dynamics*. Cambridge University Press.

https://doi.org/10.1017/jfm.2012.146 Published online by Cambridge University Press

VALLIS, G. K. & MALTRUD, M. E. 1993 Generation of mean flows and jets on a beta plane and over topography. *J. Phys. Oceanogr.* **23**, 1346–1362.

VENAILLE, A. & BOUCHET, F. 2011 Solvable phase diagrams and ensemble inequivalence for two-dimensional and geophysical flows. *J. Stat. Phys.* **143** (2), 346–380.

VENAILLE, A., LE SOMMER, J., MOLINES, J. M. & BARNIER, B. 2011*a* Stochastic variability of oceanic flows above topography anomalies. *Geophys. Res. Lett.* **38** (16611).

VENAILLE, A., VALLIS, G. K. & GRIFFIES, S. 2012 The catalytic role of beta effect in barotropization process. *J. Fluid Mech.* (submitted) arXiv:1201.0657.

VENAILLE, A., VALLIS, G. K. & SMITH, K. S. 2011*b* Baroclinic turbulence in the ocean: analysis with primitive equation and quasi-geostrophic simulations. *J. Phys. Oceanogr.* **41** (9), 1605–1623.

https://doi.org/10.1017/jfm.2012.146 Published online by Cambridge University Press